

The Al–Sb–V–Oxide System for Propane Ammoxidation: A Study of Regions of Phase Formation and Catalytic Role of Al, Sb, and V

Jerker Nilsson,* Angel R. Landa-Cánovas,† Staffan Hansen,† and Arne Andersson*

*Department of Chemical Engineering II (Chemical Technology) and †National Center for HREM, Inorganic Chemistry 2, University of Lund, Chemical Center, P.O. Box 124, S-221 00 Lund, Sweden

Received June 21, 1995; revised November 23, 1995; accepted December 28, 1995

Syntheses in the Al–Sb–V–O system, which is a candidate catalyst system for propane ammoxidation to acrylonitrile, were characterized by X-ray powder diffraction, electron diffraction, energy dispersive X-ray microanalysis, high-resolution electron microscopy, infrared spectroscopy, and catalytic measurements. The objective was to study phase formation as well as to identify the phase, or phases, which are active and selective for propane ammoxidation and to conclude about the catalytic role of the various types of metal ion centres. Calcination in air at 680°C of mixtures of Al(OH)₃, Sb₂O₃, and V₂O₅ showed the formation of α-Sb₂O₄, V₂O₅, AlVO₄, and two rutile-related phases Sb_{0.9}V_{0.9}O₄ and Al_{1-x}Sb_xO₄, 0 < x < 0.5. The latter presents a trirutile-type superlattice as shown by electron diffraction and high-resolution transmission electron microscopy. Formation of Al_{1-x}Sb_xO₄ was not observed starting from the phase composition, but required an excess of alumina (> 60 at.% Al). Without alumina in excess, Sb_{0.9}V_{0.9}O₄ is formed. Activity measurements over phases belonging to the Al–Sb–V–O system revealed that Al_{1-x}Sb_xO₄ is the most selective toward acrylonitrile formation, and it was identified as the active phase in a sample of patent type with Al : Sb : V = 21 : 5 : 1. Rationalisation of activity and selectivity data for V₂O₅, Sb₂O₄, Al₂O₃, Sb_{0.9}V_{0.9}O₄, AlVO₄, AlSbO₄, Sb_{0.9}V_{0.9}O₄/α-Sb₂O₄, β-Sb_{1.9}V_{0.1}O₄, and Al_{1-x}Sb_xO₄ showed that in oxides with vanadium, it is the V-centres which are active and determine the specific activity. To have a catalyst that is selective to acrylonitrile and to avoid combustion, it is necessary to have structurally isolated V-centres which are surrounded by Al and/or Sb.

© 1996 Academic Press, Inc.

INTRODUCTION

There is world-wide interest in the study and development of catalytic processes using alkane feedstock, replacing older technologies converting olefins and aromatics (1). One process already brought to commercial scale is butane oxidation to maleic anhydride, replacing older processes feeding butene or benzene (2). Currently, BP/SOHIO is active in developing a process for acrylonitrile manufacture from propane, as an alternative to their well-known ammoxidation process starting from propylene (3). Different types of catalysts have been patented for propane ammoxi-

ation, such as Bi–Mo–V scheelites (4) and rutiles with Sb, V, W, Mo, and Al as key elements (5). Activity data in the patents indicate the rutile system to be the most promising.

This article deals with the Al–Sb–V–oxide system and is a continuation of our previous reports on the structure and catalytic performance of the Sb–V–O subsystem (6–10). A rationalisation of the Al–Sb–V–O system for propane ammoxidation is crucial and would create a better basis for understanding and detailed investigation of the more complex multicomponent Al–Sb–(Mo, W)–V–O system.

Under oxygen-rich conditions it is known that the Al–Sb–V–O system comprises the phases AlSbO₄ (11), AlVO₄ (12), and Sb_{0.9}V_{0.9}O₄ (6, 8, 10, 13, 14) along with the simple oxides V₂O₅ (15), Sb₆O₁₃ (16), α-Sb₂O₄ (17), β-Sb₂O₄ (18), and various Al₂O₃-polymorphs (19). It has been reported that the β-Sb₂O₄ structure can accommodate vanadium and the solubility limit corresponds to the atomic ratio Sb : V = 19 : 1 (20). Moreover, some indications have been given that the rutile-related phases AlSbO₄ and SbVO₄ can form a solid solution (21). Crystalline Sb₂O₅ is formed only at high oxygen pressures (22, 23). Under reducing atmosphere there are several vanadia phases, e.g., V₄O₉, V₆O₁₃, and VO₂, which can form depending on the exact conditions (24). AlVO₃ (25) and Sb₂O₃-polymorphs (26) are other phases that are formed under reducing conditions. It has been shown that Sb_{0.9}V_{0.9}O₄ is a member of a series with the general formula Sb_{0.9}V_{0.9+x}O₄ (0 ≤ x ≤ 0.2), where the value of x increases with decrease in the partial pressure of oxygen used in the synthesis (8, 10). To the best of our knowledge there is no report in the literature on a systematic investigation of phases formed starting from oxide mixtures containing aluminum, antimony, and vanadium. One of the incentives for carrying out the present investigation was therefore to study phase formation in the Al–Sb–V–O system and to determine the performances of the pure phases in propane ammoxidation. The objective in this regard was to identify the catalytically most interesting phases and to make comparisons with a catalyst prepared according to patent procedures (5) in order to identify the active constituent or constituents.

Concerning the catalytic role of the various elements, there is general awareness in the literature that this point is not yet fully worked out. In an early work (27), it was proposed that AlSbO_4 modified with vanadium is active for the oxidative dehydrogenation of propane to propylene and that vanadium sites are needed for the consecutive transformation of propylene to acrylonitrile. However, comparison of activity data for AlSbO_4 before and after doping with vanadia ($\text{Sb} : \text{V} = 10$) suggested that vanadium sites are possibly involved in both steps (21). From comparisons with other antimonate systems which have been used for propylene ammoxidation, it was surmised that a vanadium centre is involved in the first hydrogen abstraction from propane and that Sb^{5+} is the nitrogen insertion element (28). Some support for the latter hypothesis was found in our previous investigation of the Sb-V-O system for propane ammoxidation, where the active phase was identified as $\text{Sb}_{0.9}\text{V}_{0.9}\text{O}_4$ enriched with antimony at the surface (7, 9). In a more recent investigation of the Sb-V-O system for propylene ammoxidation (29), however, data were obtained showing that surface enrichment with antimony on $\text{Sb}_{0.9}\text{V}_{0.9}\text{O}_4$ results in less formation of degradation products. This finding suggests that the main role of antimony can be to poison and dilute the active vanadia sites to a suitable level. In this regard, another objective of the present work was to con-

clude about the catalytic role of vanadium, antimony, and aluminium sites. This was achieved by comparing the catalytic behavior of prepared oxide phases, having different combinations of V, Sb, and Al in the lattice and of which several have the rutile type of structure.

EXPERIMENTAL

Preparation of Samples

The regions of phase formation in the Al-Sb-V-O system under air at atmospheric pressure were investigated starting from $\text{Al}(\text{OH})_3$ (Riedel-de-Haën, pA), Sb_2O_3 (Merck, pA), and V_2O_5 (Riedel-de-Haën, pA). Weighed amounts (specified in Fig. 1) of the oxides were mixed and ground together in an agate mortar and were then heated at 680°C for 4 days with one intermittent grinding. The heating rate from ambient temperature up to 680°C was $10^\circ\text{C}/\text{min}$. To enhance crystal growth, the temperature for synthesis was selected close to the upper limit, which according to patents is preferable for this type of catalyst (5). Some samples were calcined at 900 and 1000°C .

After having determined the phases formed in the Al-Sb-V-O system, the pure phases present were synthesised in air for use in propane ammoxidation. V_2O_5 was prepared

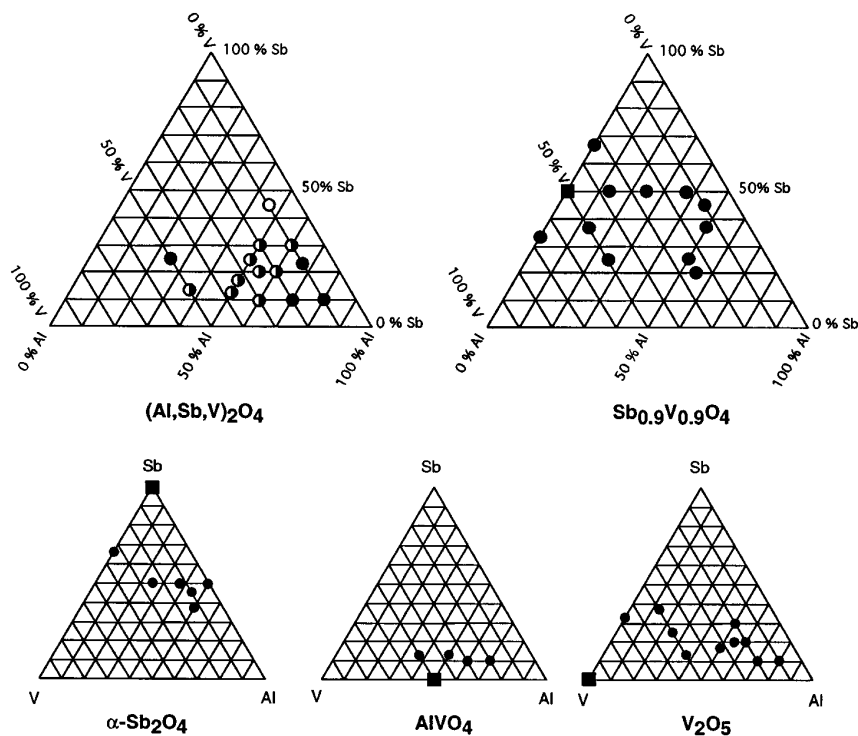


FIG. 1. Fields of formation (at.%) in air at 680°C of crystalline phases in Al-Sb-V-O syntheses as determined by powder X-ray diffraction. The circles, in all cases, are marked at the starting composition which was used for the synthesis. For $(\text{Al, Sb, V})_2\text{O}_4$, a filled circle denotes $(\text{Al, Sb, V})_2\text{O}_4$ (I), an unfilled circle denotes $(\text{Al, Sb, V})_2\text{O}_4$ (II), and a half-filled circle denotes the presence of both $(\text{Al, Sb, V})_2\text{O}_4$ (I) and $(\text{Al, Sb, V})_2\text{O}_4$ (II). A square indicates an oxide phase observed and with the metal composition given by the triangle axes.

by calcining NH_4VO_3 at 450°C in flowing air for 2 h. $\alpha\text{-Sb}_2\text{O}_4$ was prepared by heating Sb_2O_3 at 800°C for 30 h. $\gamma\text{-Al}_2\text{O}_3$ (pA) was supplied by BDH. The synthesis of $\text{Sb}_{0.9}\text{V}_{0.9}\text{O}_4$ was made from an equimolar mixture of V_2O_5 and Sb_2O_3 , which was calcined at 800°C for 2.5 h. AlVO_4 was prepared from stoichiometric amounts of $\text{Al}(\text{OH})_3$ and V_2O_5 , which were heated at 670°C for 4 days with one intermittent grinding. A rutile phase $(\text{Al}, \text{Sb}, \text{V})_2\text{O}_4$ with all three metals was made starting from a mixture of $\text{Al}(\text{OH})_3$, Sb_2O_3 , and V_2O_5 (atomic ratios $\text{Al} : \text{Sb} : \text{V} = 9 : 9 : 2$), which was heated at 900°C for 6 days with two intermittent grindings.

Some additional phases that were not formed in the Al-Sb-V-O system at 680°C were prepared as well. $\beta\text{-Sb}_2\text{O}_4$ was obtained by heating in air Sb_2O_3 at 1000°C for 5 days followed by rapid cooling to room temperature. Vanadium-doped $\beta\text{-Sb}_2\text{O}_4$ was made from an intimate mixture of Sb_2O_3 and V_2O_5 ($\text{Sb} : \text{V} = 19 : 1$), which was calcined in air at 850°C for 4 h. AlSbO_4 was prepared starting from a stoichiometric mixture of $\text{Al}(\text{OH})_3$ and Sb_2O_3 , which was heated in air at 1150°C for 24 h.

A catalyst sample with $\text{Al} : \text{Sb} : \text{V} = 21.3 : 5.0 : 1.0$ was prepared closely following a procedure that is described in some examples of the patents (5). Thus, 5.4 g of NH_4VO_3 was dissolved in 150 ml hot water and then 33.6 g of Sb_2O_3 was added. The slurry was boiled under reflux for 4 days. Separately, 76.713 g of $\text{Al}(\text{OH})_3$ was added to 200 ml cold water, to which 23 g of acetic acid had been added as 10 wt. % solution. This mixture was stirred until gelling, which took approximately 3 h. The alumina gel was now added to the refluxed slurry with stirring, followed by drying, first on a hot plate, then at 90°C for 2 days, and finally at 120°C for 12 h. Precalcination of the solid material was performed in flowing air for 5 h at 350°C before crushing and sieving. A final calcination of the 150- to $425\text{-}\mu\text{m}$ fraction of particle size was performed in flowing air at 610°C for 3 h.

An $\text{AlVO}_4/\text{Al}_2\text{O}_3$ sample with the synthesis ratio $\text{Al} : \text{V} = 7.5 : 1.0$ was prepared following the procedure used for preparation of the patent-type of catalyst, with the exception that no Sb_2O_3 was added and an additional calcination was made at 670°C for 16 h. Moreover, an $\text{Sb}_{0.9}\text{V}_{0.9}\text{O}_4/\alpha\text{-Sb}_2\text{O}_4$ sample with the nominal ratio $\text{Sb} : \text{V} = 2 : 1$ was prepared as previously described (7).

For each of the pure phases which were used as catalysts the JCPDS file (30) or another reference to the literature for diffraction data is given in Table 1.

Characterisation of Samples

For X-ray powder diffraction, the samples were crushed and mounted on adhesive tape. Films were recorded using a Guinier-Hägg focusing camera with $\text{CuK}\alpha_1$ radiation (wavelength 1.54056 \AA) and with Si as internal standard (cubic unit cell constant 5.43088 \AA).

Energy dispersive X-ray microanalysis was carried out in a transmission electron microscope JEM-2000FX fitted

TABLE 1
Specific Surface Area of Catalyst Samples

Sample	Reference ^a	BET area (m ² /g)
V_2O_5	JCPDS 41-1426	5.1
$\gamma\text{-Al}_2\text{O}_3$	JCPDS 10-425	277.6
$\alpha\text{-Sb}_2\text{O}_4$	JCPDS 11-694	0.6
$\beta\text{-Sb}_2\text{O}_4$	JCPDS 17-620	0.2
$\beta\text{-Sb}_{1.9}\text{V}_{0.1}\text{O}_4$	Ref. (20)	1.2
$\text{Sb}_{0.9}\text{V}_{0.9}\text{O}_4$	Ref. (6)	2.0
$\text{Sb}_{0.9}\text{V}_{0.9}\text{O}_4/\alpha\text{-Sb}_2\text{O}_4$ with $\text{Sb} : \text{V} = 2 : 1$		3.6
AlVO_4	JCPDS 39-276	0.2
$\text{AlVO}_4/\text{Al}_2\text{O}_3$ with $\text{Al} : \text{V} = 7.5 : 1.0$		146.0
AlSbO_4	JCPDS 4-564	4.2
$(\text{Al}, \text{Sb}, \text{V})_2\text{O}_4^b$	This work, Table 4	1.3
Patent-type with $\text{Al} : \text{Sb} : \text{V} = 21.3 : 5.0 : 1.0$		157.4

^a Reference to the JCPDS file in Ref. (30) or other literature for XRD or neutron diffraction data of the pure phase.

^b Sample JN126 in Table 3. The metal atomic ratio which was charged for the synthesis was $\text{Al} : \text{Sb} : \text{V} = 9 : 9 : 2$.

with a Link AN10000 analysis system. The phases were first identified by electron diffraction and thin edges were then analysed using a beam approximately 500 \AA in diameter and an acceleration voltage of 200 kV .

High-resolution transmission electron microscopy was performed in a JEM-4000EX instrument operated at 400 kV and possessing a structural resolution of 1.6 \AA . Samples were lightly ground in methanol and the dispersion was then transferred to copper grids covered with a holey carbon film. In the microscope, thin crystals positioned over the holes in the carbon film were examined by diffraction and imaging techniques.

BET surface areas were determined with a Micromeritics Flowsorb 2300 instrument, applying adsorption of N_2 at liquid N_2 temperature. The samples were degassed at 350°C . Specific surface areas of the samples used as catalysts are included in Table 1.

FTIR spectra were recorded on a Nicolet 20 SXC spectrometer equipped with a CsI beamsplitter. Disks containing 3 mg sample and 200 mg KBr were pressed. Spectra were recorded in an atmosphere of dry air. The resolution was 2 cm^{-1} and 1000 scans were averaged.

Raman measurements were performed with a Bruker IFS 66 FTIR spectrometer equipped with an FRA 106 Raman device. A low power diode pumped Nd:YAG laser with an excitation line at 1046 nm and a liquid nitrogen-cooled germanium diode detector were used. Measurements were carried out under ambient conditions on undivided catalyst particles in 5-mm NMR tubes. The laser power was usually set at 100 mW and the resolution was 8 cm^{-1} . Backscattering at 180° was measured and 4000 scans were averaged.

XPS measurements were performed with a Kratos XSAM 800 instrument using MgK α X-ray radiation (1253.6 eV). The sample was attached to the sample holder with double-sided tape. Charging effects were overcome by mixing the sample with acetylene black (Carbon Philblack 1-ISAF from Nordisk Philblack AB). The C 1s signal was set to a position of 284.3 eV.

The activity measurements were performed using an isothermal plug-flow reactor made from glass. Conversion and selectivities were studied varying the amount of catalyst at constant flow rate. Dilution of the catalyst samples with quartz grains was necessary to have isothermal conditions. Dead volumes were reduced using glass beads, and hot zones in the tubing between the reactor and the analysis equipment were avoided to have negligible contribution from homogeneous conversions. The reactor temperature was 480°C and the composition of the feed expressed as the mole ratio propane: ammonia: oxygen: water vapor: nitrogen was 2:2:4:1:5. Propane and the products propylene, acrylonitrile, acetonitrile, ethylene, methane, CO, and CO₂ were analysed on a GC that was equipped with a Porapak Q column, a sample valve, an FID detector, and a methaniser for analysis of the carbon oxides. Analyses of ammonia conversion and formation of HCN were performed using titrimetric methods (31). It was verified that the carbon balance was complete.

RESULTS

Phases in the Al-Sb-V-O System

The samples synthesised in air at 680°C, from mixtures of Al(OH)₃, Sb₂O₃, and V₂O₅ in various ratios, were analysed with X-ray powder diffraction. Crystalline α -Sb₂O₄, AlVO₄, and V₂O₅ and three rutile-related phases Sb_{0.9}V_{0.9}O₄, (Al, Sb, V)₂O₄ (I), and (Al, Sb, V)₂O₄ (II) were identified (see Table 2). The rutile-like phase with the largest unit cell is Sb_{0.9}V_{0.9}O₄, while AlSbO₄ has the smallest cell volume. The latter phase does not form in the pure Al-Sb-O system at 680°C (11), but when vanadia is present a phase designated (Al, Sb, V)₂O₄ (I) with similar unit cell parameters can form

TABLE 2

Unit Cell Parameters for Rutile-Related Phases in the Al-Sb-V-O Syntheses as Determined by Powder X-Ray Diffraction

Phase	<i>a</i> (Å) ^a	<i>c</i> (Å) ^a
AlSbO ₄ ^b	4.52	2.97
(Al, Sb, V) ₂ O ₄ (I)	4.51–4.52	2.95–2.97
(Al, Sb, V) ₂ O ₄ (II)	4.54–4.57	3.00–3.01
Sb _{0.9} V _{0.9} O ₄	4.62–4.63	3.04–3.03

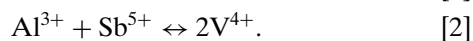
^a The estimated standard deviations obtained in the least-squares refinements were ≤ 0.002 Å.

^b Not formed in air at 680°C.

at the present temperature. The phase designated (Al, Sb, V)₂O₄ (II) exhibits an intermediate unit cell size. No trace of diffraction lines from Al₂O₃ was detected by this method, even in a sample of pure alumina.

Figure 1 shows the phases present for the different starting compositions. It can be seen that α -Sb₂O₄ and AlVO₄ are formed more or less close to their ideal metal stoichiometry. V₂O₅ is formed in the Sb-poor half of the triangle. This behavior is compatible with the fact that 680°C is close to the temperature where AlVO₄ decomposes into V₂O₅ and X-ray amorphous Al₂O₃ (12). Formation of the rutile Sb_{0.9}V_{0.9}O₄ is observed over a wide range of starting compositions, while (Al, Sb, V)₂O₄ is exclusively observed in the Al-rich part of the system. It appears that the formation of Sb_{0.9}V_{0.9}O₄ is kinetically favoured and that a large excess of alumina, > 60 at. % Al, is required to obtain (Al, Sb, V)₂O₄ as the only rutile-phase or phases. It is noteworthy that (Al, Sb, V)₂O₄ (I) and (Al, Sb, V)₂O₄ (II) often occur together and that, in some cases, all three rutiles are present in the same sample.

To investigate the nature of vanadium substitution in AlSbO₄, three representative samples synthesised under various conditions and containing the (Al, Sb, V)₂O₄ phases were selected using the available powder diffraction data (see Table 3). Crystals of (Al, Sb, V)₂O₄ in each sample were first identified by electron diffraction and were then investigated using energy dispersive X-ray analysis. A scatter plot of the analysis results is in Fig. 2. The two most simple substitution mechanisms for the vanadium in AlSbO₄ are



It is evident from Fig. 2 that the observed data points fall along the line that corresponds to mechanism [1] and not the one generated by mechanism [2]. Despite a slight overestimation of the Sb content, a solid solution series can be formulated as Al_{1-x}Sb_xV_xO₄ with 0 < *x* < 0.5. The phase with the larger unit cell, (Al, Sb, V)₂O₄ (II), is richer in vanadium than (Al, Sb, V)₂O₄ (I), which has a smaller unit cell (see Table 2 and 4). Shannon (32) reported the ionic radii Al³⁺ 0.54, Sb⁵⁺ 0.60, V³⁺ 0.64, and V⁴⁺ 0.58 Å, which fit well with the observed unit cell expansion when Al³⁺ in AlSbO₄ is substituted by larger amounts of V³⁺ as in (Al, Sb, V)₂O₄ (II). This phase, which is the major rutile-related phase in sample JN51 (Table 3), exhibits an approximate composition of Al_{0.5}Sb_{1.0}V_{0.5}O₄, while the composition of (Al, Sb, V)₂O₄ (I) in the sample JN163 is approximately Al_{0.8}Sb_{1.0}V_{0.2}O₄. The rutile-related phase in JN163 has previously been subjected to energy dispersive X-ray analysis using a scanning electron microscope with similar result (33). For the sample containing both (Al, Sb, V)₂O₄ phases (JN126 in Table 3), the whole range of compositions is observed, as is obvious from Fig. 2. It is thus clear that the composition of (Al, Sb,

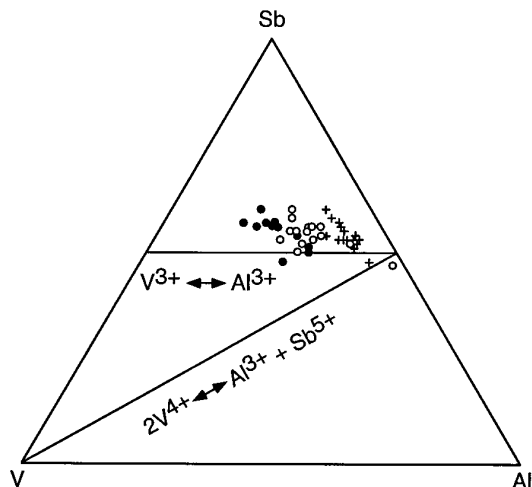


FIG. 2. Energy dispersive X-ray microanalyses of rutile-related (Al, Sb, V)₂O₄ crystals in the three representative samples presented in Table 3. Cross symbol, JN163; open circle, JN126; closed circle, JN51.

V)₂O₄ in this sample is not homogeneous, but it varies from crystal to crystal. A comparison of the field of formation for (Al, Sb, V)₂O₄ in Fig. 1 with its range of composition in Fig. 2 shows that at 680°C (Al, Sb, V)₂O₄ is not formed in syntheses that starts from compositions corresponding to the phase compositions. Instead, Sb_{0.9}V_{0.9}O₄ is formed. The formation of (Al, Sb, V)₂O₄ requires a large excess of alumina in the starting mixture of oxides.

Electron diffraction and X-ray microanalyses of Al–Sb–V–O syntheses identified crystal aggregates, like the one in Fig. 3, as δ -Al₂O₃. This polymorph of alumina exhibits a threefold spinel supercell with the lattice parameters $a = b = 7.94$ Å and $c = 23.50$ Å (34). It thus is closely related to γ -Al₂O₃, which exhibits the basic spinel-type cell. The threefold superlattice is for example evident in Fig. 3b from the presence of two weak spots between the origin spot (central beam) and the reflection 0 0 12 (0 0 4 in the spinel). The individual crystals are only 5–10 nm in size, which explains why no alumina is detectable with X-ray methods. The alumina particles are nevertheless crystalline, as revealed by electron diffraction. Therefore, a sample that

TABLE 4
X-Ray Powder Diffraction Data for (Al, Sb, V)₂O₄ Phases; Interplanar Spacings (d) and Visually Estimated Relative Intensities (I_{rel})

hkl	I_{rel}	(Al, Sb, V) ₂ O ₄ (I) ^a		(Al, Sb, V) ₂ O ₄ (II) ^b	
		d_{obs} (Å)	d_{calc} (Å)	d_{obs} (Å)	d_{calc} (Å)
1 1 0	5	3.202	3.198	3.232	3.231
1 0 1	4	2.487	2.485	2.517	2.514
2 0 0	2	2.261	2.262	2.280	2.284
1 1 1	2	2.179	2.178	2.203	2.202
2 1 0	1	2.022	2.023	nm ^c	2.043
2 1 1	4	1.673	1.673	1.691	1.691
2 2 0	1	1.599	1.599	nm ^c	1.615
0 0 2	1	1.487	1.487	1.504	1.505
3 1 0	2	1.431	1.430	1.445	1.445
3 0 1, 1 1 2	3	1.345	1.345; 1.349	1.365	1.359; 1.364
2 0 2	1	nm ^c	1.243	1.256	1.257

^a JN163 \approx Al_{0.8}Sb_{1.0}V_{0.2}O₄; $a = 4.5233(4)$ Å, $c = 2.9746(5)$ Å.

^b JN51 \approx Al_{0.5}Sb_{1.0}V_{0.5}O₄; $a = 4.569(2)$ Å, $c = 3.010(1)$ Å.

^c Not measured.

appears to be monophasic according to its powder diffraction pattern can contain large amounts of alumina. Moreover, the starting metal composition is of little use when determining the actual composition of phases formed, because antimony(III) oxides are known to be volatile and at higher temperatures also V₂O₅ exhibits a certain vapor pressure. Consequently, X-ray microanalysis of individual crystals is necessary for determination of the metal composition of the phases that are formed in this type of calcination, i.e., in an open system as is common procedure in catalyst manufacture (5).

The fact that the δ -Al₂O₃ aggregates, which are composed of large numbers of crystals, give spot diffraction patterns such as the ones in Figs. 3a and 3b indicates that the crystals are well aligned. The observed texture of the δ -Al₂O₃ indicates its formation by topotactic decomposition from a well-crystallised precursor, possibly Al(OH)₃ or AlO(OH).

Electron microscopy of the rutile-related Sb_{0.9}V_{0.9}O₄ and (Al, Sb, V)₂O₄ reveals well-formed crystals with morphologies that are typical for rutile-type minerals (see

TABLE 5
Rutile-Related (Al, Sb, V)₂O₄ Phases in Selected Samples from the Al–Sb–V–O Syntheses According to Powder X-Ray Diffraction

Sample	Starting metal composition	Time of heating (days)	Heating temperature (°C)	Phases
JN163	Al _{0.5} Sb _{1.0} V _{0.5}	4	1000	(Al, Sb, V) ₂ O ₄ (I) ^a
JN126	Al _{0.9} Sb _{0.9} V _{0.2}	6	900	(Al, Sb, V) ₂ O ₄ (I); (Al, Sb, V) ₂ O ₄ (II)
JN51	Al _{1.2} Sb _{0.6} V _{0.2}	4	680	(Al, Sb, V) ₂ O ₄ (II) ^b ; trace (Al, Sb, V) ₂ O ₄ (I)

^a Composition of (Al, Sb, V)₂O₄ (I) as determined by EDX analysis \approx Al_{0.8}Sb_{1.0}V_{0.2}O₄.

^b Composition of (Al, Sb, V)₂O₄ (II) as determined by EDX analysis \approx Al_{0.5}Sb_{1.0}V_{0.5}O₄.

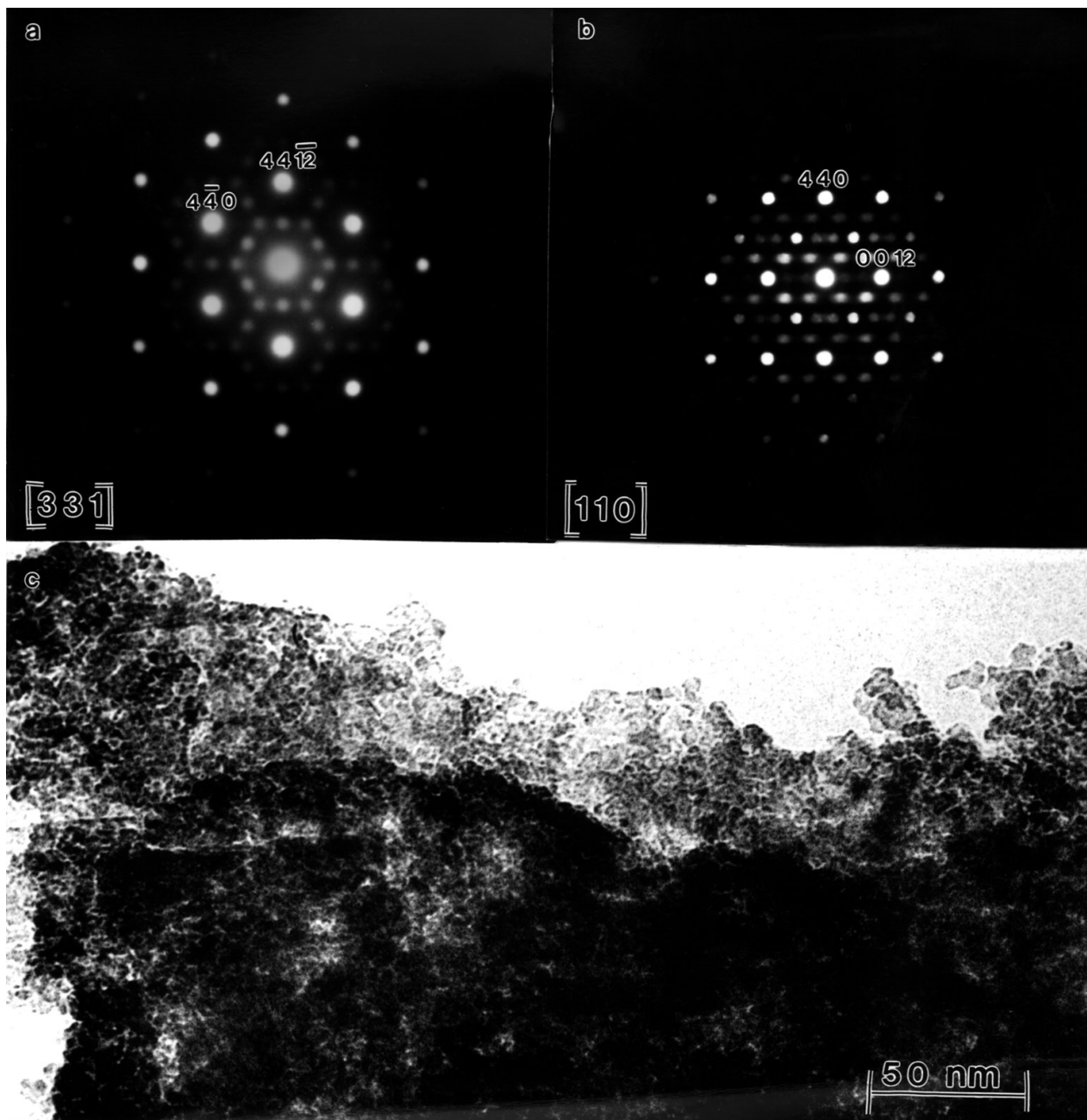


FIG. 3. Electron microdiffraction patterns of δ - Al_2O_3 in a sample from the Al-Sb-V-O syntheses. In (a) the electron beam is along the crystallographic direction $[331]$ and in (b) along $[110]$. (c) Transmission electron micrograph of a topotactic δ - Al_2O_3 aggregate.

Figs. 4a and 5b). Crystals of $(\text{Al, Sb, V})_2\text{O}_4$ are often dominated by $\{110\}$ prism faces, but recurring surface steps produces a distinct obelisk habit.

As can be seen in the electron diffraction patterns in Figs. 4b and 5a, and as we have reported in more detail elsewhere (10, 33), the phases $\text{Sb}_{0.9}\text{V}_{0.9}\text{O}_4$ and $(\text{Al, Sb, V})_2\text{O}_4$ both exhibit rutile-related structures. With powder X-ray diffraction using the Guinier technique only the basic rutile-type reflections are observed. These reflections

can all be indexed using a tetragonal cell; a_{rutile} , c_{rutile} , and the extinct reflections are compatible with the space group $P4_2/mnm$. With selected area electron diffraction, on the other hand, two very different superlattices are observed; $\text{Sb}_{0.9}\text{V}_{0.9}\text{O}_4$ exhibits a 32-fold supercell ($a = 2\sqrt{2} \cdot a_{\text{rutile}}$, $b = 2\sqrt{2} \cdot b_{\text{rutile}}$, and $c = 4 \cdot c_{\text{rutile}}$), while both $(\text{Al, Sb, V})_2\text{O}_4$ (I) and $(\text{Al, Sb, V})_2\text{O}_4$ (II) exhibit very similar patterns with a 3-fold supercell (tetragonal, trirutile-type: $a = a_{\text{rutile}}$ and $c = 3 \cdot c_{\text{rutile}}$). Both the 32-fold and the 3-fold types of super-

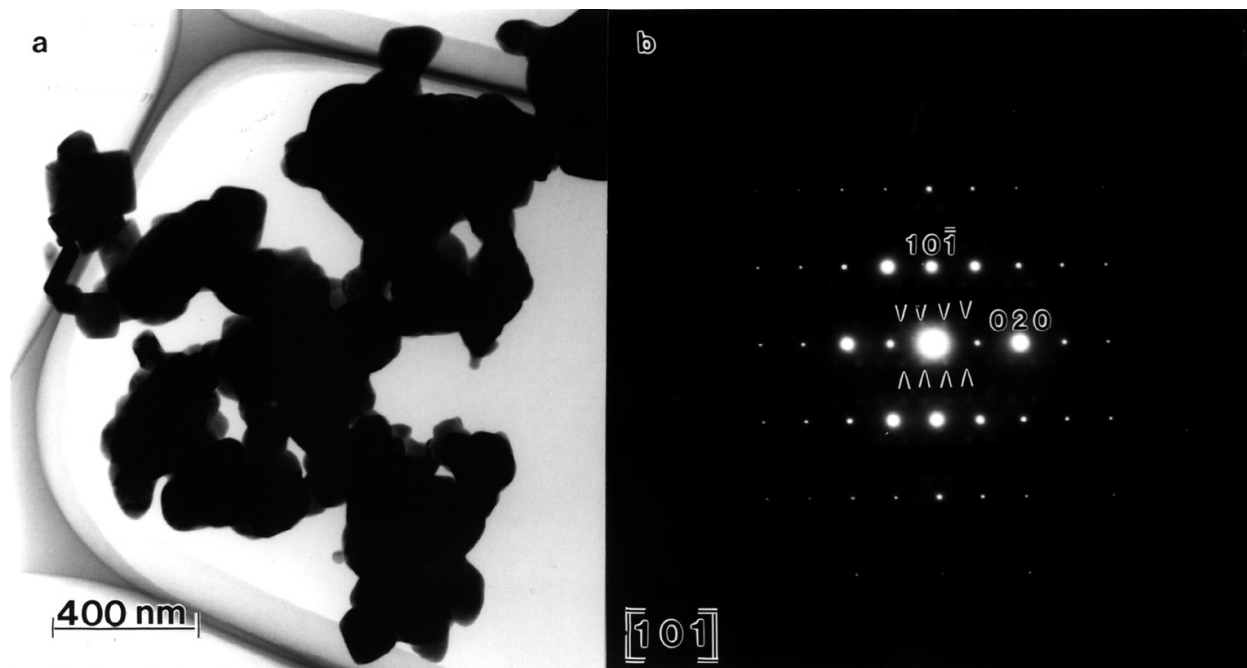


FIG. 4. The phase $\text{Sb}_{0.9}\text{V}_{0.9}\text{O}_4$ in a sample from the Al-Sb-V-O syntheses. (a) Transmission electron micrograph of crystal aggregates. (b) Selected area electron diffraction pattern with zone axis $[101]$. Strong basic reflections are indexed using the rutile-type unit cell and weak superlattice reflections are marked by arrows.

structure are better described as incommensurably modulated crystal structures (10, 33), but in the present context the important thing is that the two phases can readily be distinguished by electron diffraction. Note that formulas based on four oxygen atoms correspond to the content of the basic rutile unit cell.

The trirutile structure is usually found in AB_2O_6 materials (where A and B are different metal ions) and is due to ABBABBA metal ordering along z in the basic rutile structure. This type of metal ordering is directly observable in the atomic resolution micrograph shown in Fig. 5c. Calculations (33) have shown that the white dots correspond to metal positions. In certain areas, the metal ordering is observed as sequences big dot/big dot/small dot or small dot/small dot/big dot along z . However, it is clear from the image that the cation ordering is far from perfect on the unit cell level.

Propane Ammoxidation

Ammoxidation of propane was studied over the samples listed in Table 1. The initial reaction rate and the selectivities to the C_3 products propylene and acrylonitrile at 5, 10, and 15% of propane conversion are presented in Figs. 6, 7, and 9. Additionally, acetonitrile, HCN, CO, and CO_2 were formed as well as minor amounts of ethylene and methane, which all are degradation products (C_2 - C_1). The conversion levels were selected to highlight the initial product distribution as well as the ability of the catalyst to transform the

formed propylene further to acrylonitrile. The latter point is important, considering that it has been shown that propylene is a major intermediate from propane to acrylonitrile (7, 9, 27, 31).

Ammoxidation over oxides with one metal cation. Figure 6 shows the data for V_2O_5 , $\gamma\text{-Al}_2\text{O}_3$, $\alpha\text{-Sb}_2\text{O}_4$, and $\beta\text{-Sb}_2\text{O}_4$. The data sets for the two antimony oxides are not complete, because their low activity per volume of catalyst did not allow measurement above 5–10% conversion. It is obvious that vanadia is the most active of the oxides and also is the most selective to propylene formation at low conversion levels. The antimony oxides are considerably less active, but present some initial selectivity to propylene, whereas $\gamma\text{-Al}_2\text{O}_3$ has very low activity expressed per unit surface area of catalyst and is selective to degradation products. Considering the variations with propane conversion of the selectivities to propylene and acrylonitrile, it is apparent that the propylene formed rapidly degrades on the antimony oxide surface, while the degradation is somewhat less on vanadia. However, at 35% propane conversion on the vanadia, the selectivity to propylene had decreased to about 10%, while the selectivity to acrylonitrile had not changed much compared to the data in Fig. 6 for 10 and 15% conversion. Thus, neither vanadia nor antimony oxide are able to transform the intermediate propylene selectively to acrylonitrile and for both oxides the selectivity to acrylonitrile formation is not more than 10% at 5–15% propane conversion.

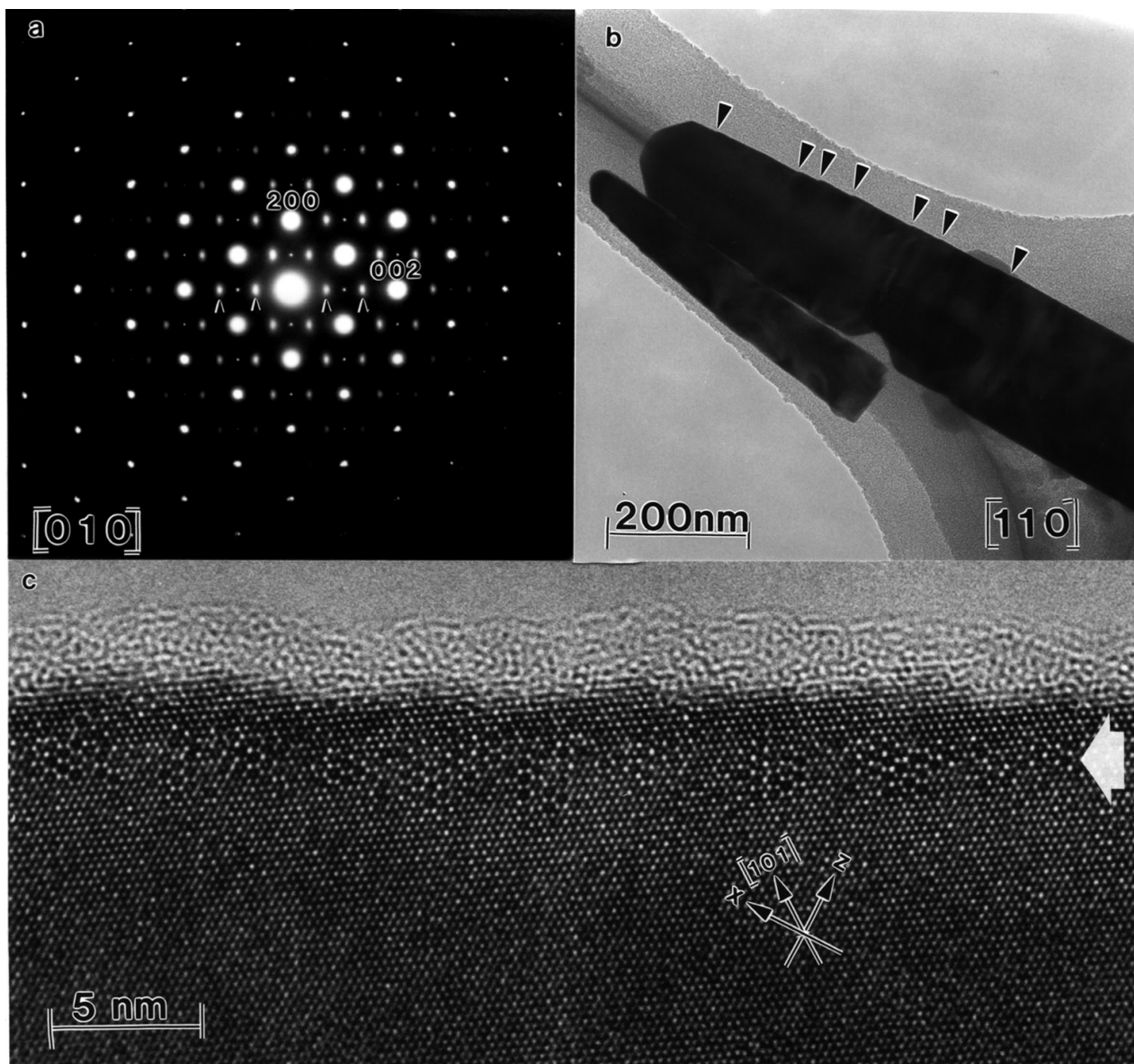


FIG. 5. $(\text{Al, Sb, V})_2\text{O}_4$ in a sample from the Al-Sb-V-O syntheses. (a) Selected area electron diffraction pattern with zone axis $[010]$. Circular basic reflections are indexed using the rutile cell and elongated superlattice reflections are marked by arrows. (b) Electron micrograph of two crystals with steps (arrowheads) on $\{110\}$ surfaces. (c) Atomic resolution micrograph taken along $[010]$ showing a trirutile-type cation-ordering, which is best seen close to the edge of the crystal in the horizontal area marked by a thick arrow (right). If the image is viewed at low angle along the x -direction (thin arrow), the ordering can be seen to extend all over the crystal.

Ammonoxidation over oxides with two metal cations. Conversion data over $\text{Sb}_{0.9}\text{V}_{0.9}\text{O}_4$, AlVO_4 in unsupported and Al_2O_3 -supported form, and AlSbO_4 are shown in Fig. 7. AlSbO_4 is less active than the α - and β -polymorphs of Sb_2O_4 (cf. Fig. 6) but shows comparable selectivity to propylene and acrylonitrile at low conversion, indicating that an antimony moiety is the active centre in AlSbO_4 . This conclusion is supported by fact that alumina centres in γ - Al_2O_3 have low activity and selectivity to propylene, which is apparent from Fig. 6.

Compared to AlSbO_4 , both $\text{Sb}_{0.9}\text{V}_{0.9}\text{O}_4$ and AlVO_4 are considerably more active and more selective to acrylonitrile formation. Moreover, compared to V_2O_5 (Fig. 6) they are more selective to acrylonitrile and show similar or even higher selectivity values for propylene formation. It should be noticed, however, that the decrease in the selectivity to propylene formation with increased propane conversion does not go with a corresponding increase in the selectivity to acrylonitrile. This shows that the formed propylene degrades on $\text{Sb}_{0.9}\text{V}_{0.9}\text{O}_4$ and AlVO_4 .

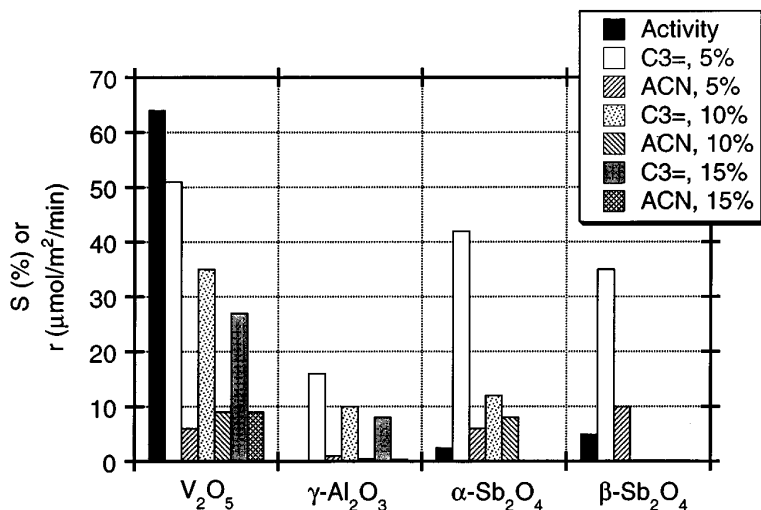


FIG. 6. Propane ammoxidation over V_2O_5 , $\gamma\text{-Al}_2O_3$, $\alpha\text{-Sb}_2O_4$ and $\beta\text{-Sb}_2O_4$. Initial reaction rate per surface area unit of catalyst (r) and selectivities (S) for propylene (C3=) and acrylonitrile (ACN) formations at 5, 10, and 15% of propane conversion.

The performance of unsupported and Al_2O_3 -supported $AlVO_4$ is rather similar, indicating that the importance of particle size of the $AlVO_4$ phase is limited. Considering the large difference in specific surface area between the two samples (cf. Table 1), evidently the acrylonitrile once formed is a stable product. Of the samples with two metal cations, the $AlVO_4/Al_2O_3$ sample seems the most interesting to consider in some more detail, because at 15% propane conversion the selectivity to propylene is still more than 40%. Data to about 55% conversion are plotted in Fig. 8, showing a sharp drop in the selectivity to propylene with increase in propane conversion. Simultaneously, there is only a modest increase in selectivity to acrylonitrile. For 55% propane conversion, the selectivity to propylene and

nitrile are 10 and 20%, respectively, and the yield to acrylonitrile is 11%. Considering that the inlet feed composition was stoichiometric for acrylonitrile formation, a propane conversion higher than 55% was not reached due to combustion and depletion of the stream with oxygen (conversion 100%) and ammonia (conversion 80%). Apparently, $AlVO_4$ is not a prime catalyst for propane ammoxidation.

Ammoxidation over oxides with structurally isolated vanadium cations. Data for $Sb_{0.9}V_{0.9}O_4$ with excess $\alpha\text{-Sb}_2O_4$ ($Sb:V=2:1$) and $\beta\text{-Sb}_{1.9}V_{0.1}O_4$ are presented in Fig. 9. The latter sample is a solid solution, where 5% of the cations in the $\beta\text{-Sb}_2O_4$ basic structure are substituted for vanadium ions (20). In case of the former sample, migration

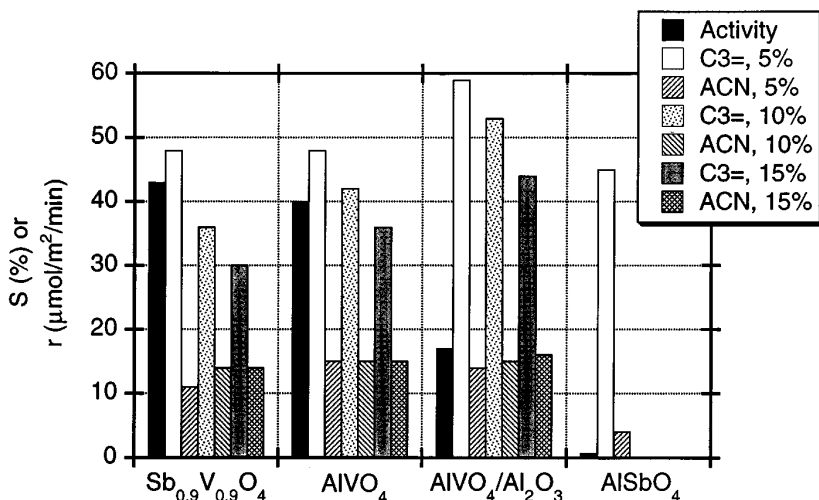


FIG. 7. Propane ammoxidation over $Sb_{0.9}V_{0.9}O_4$, $AlVO_4$, $AlVO_4/Al_2O_3$, and $AlSbO_4$. Initial reaction rate per surface area unit of catalyst (r) and selectivities (S) for propylene (C3=) and acrylonitrile (ACN) formations at 5, 10, and 15% of propane conversion.

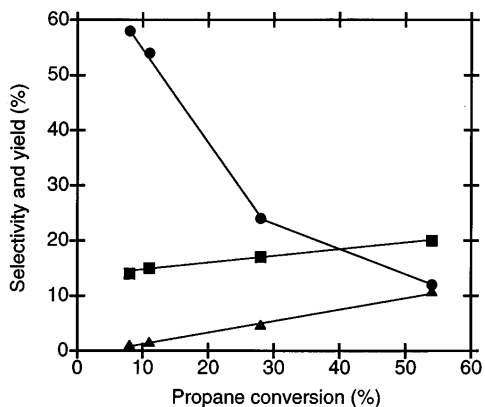


FIG. 8. Selectivity to propylene (circles) and acrylonitrile (squares) and yield for acrylonitrile formation (triangles) as a function of propane conversion over $\text{AlVO}_4/\text{Al}_2\text{O}_3$.

of antimony species from the excess $\alpha\text{-Sb}_2\text{O}_4$ over the surface of $\text{Sb}_{0.9}\text{V}_{0.9}\text{O}_4$ has been observed to occur during ammoxidation, resulting in dilution of vanadium centres at the surface (7, 9, 29). Comparison of the data in Fig. 9 for these samples with the data in Figs. 6 and 7 for the other oxides shows the $\text{Sb}_{0.9}\text{V}_{0.9}\text{O}_4/\alpha\text{-Sb}_2\text{O}_4$ and $\beta\text{-Sb}_{1.9}\text{V}_{0.1}\text{O}_4$ samples to be more selective to acrylonitrile formation. Moreover, as the selectivity to propylene decreases with increase in propane conversion, there is a concurrent increase of the selectivity to acrylonitrile. Over both samples the selectivity to acrylonitrile is more than 30% at 15% propane conversion. This is a substantial improvement compared to the corresponding selectivity over $\text{Sb}_{0.9}\text{V}_{0.9}\text{O}_4$, AlVO_4 and the simple oxides, which is only half or less.

Ammoxidation over oxides with three metal cations. Figure 9 shows data as well for two Al-Sb-V-oxide samples, i.e., the rutile sample $(\text{Al, Sb, V})_2\text{O}_4$ (JN126), and the preparation of patent-type with the atomic ratio $\text{Al}:\text{Sb}:\text{V} = 21:5:1$. As for the $\text{Sb}_{0.9}\text{V}_{0.9}\text{O}_4/\alpha\text{-Sb}_2\text{O}_4$ and $\beta\text{-Sb}_{1.9}\text{V}_{0.1}\text{O}_4$ samples, $(\text{Al, Sb, V})_2\text{O}_4$ is, compared with the samples dealt with in Figs. 6 and 7, more selective to acrylonitrile formation. This function seems linked to a more facile transformation of intermediate propylene to the nitrile. The selectivity data in Fig. 9 are similar for $(\text{Al, Sb, V})_2\text{O}_4$ and the Al-Sb-V-oxide of patent-type, though the latter sample is less active per unit surface area of sample. This comparison suggests that $(\text{Al, Sb, V})_2\text{O}_4$ is the active and selective constituent in the sample of patent-type and that the excess alumina in the latter functions as catalyst support, which for the present case is not completely covered with the active phase. Further evidence for this inference is given in Fig. 10, which shows that the variations with propane conversion of the selectivities to propylene and acrylonitrile as well as the yield to acrylonitrile over $(\text{Al, Sb, V})_2\text{O}_4$ and the patent-type catalyst follow the same graphs. The selectivity to acrylonitrile passes through a maximum of about 45% at 30% propane conversion, while the corresponding yield levels off at 20% for 50–60% conversion. Further conversion was limited by the complete consumption of the oxygen in the feed, but ammonia was still breaking through (conversion 75%).

Catalyst Characterisation

Al-Sb-V-O catalyst of patent-type. The only phase observed by powder X-ray diffraction in the Al-Sb-V-O catalyst of patent-type was $\alpha\text{-Sb}_2\text{O}_4$. In the electron microscope

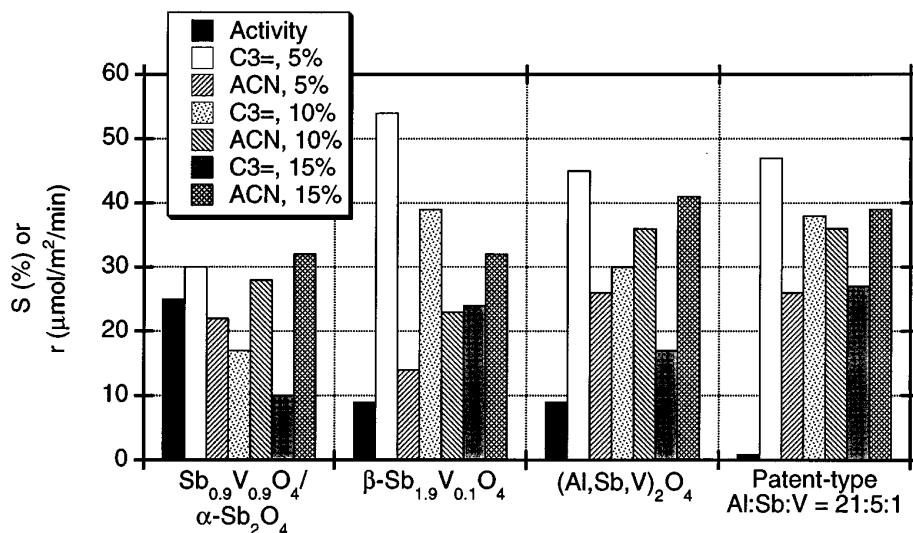


FIG. 9. Propane ammoxidation over $\text{Sb}_{0.9}\text{V}_{0.9}\text{O}_4/\alpha\text{-Sb}_2\text{O}_4$, $\beta\text{-Sb}_{1.9}\text{V}_{0.1}\text{O}_4$, $(\text{Al, Sb, V})_2\text{O}_4$, and patent-type Al-Sb-V-oxide. Initial reaction rate per surface area unit of catalyst (r) and selectivities (S) for propylene ($\text{C}_3=$) and acrylonitrile (ACN) formations at 5, 10, and 15% of propane conversion.

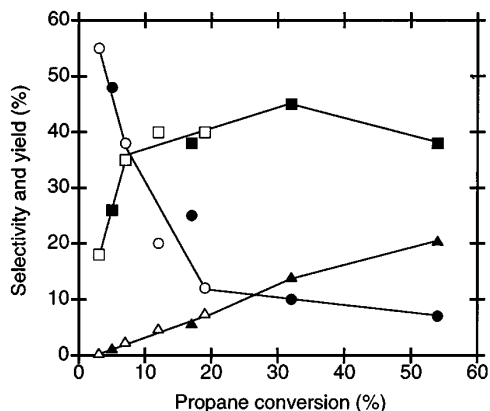


FIG. 10. Selectivity to propylene (circles) and acrylonitrile (squares) and yield for acrylonitrile formation (triangles) as a function of the conversion of propane over $\text{Al}_{0.9}\text{Sb}_{0.9}\text{V}_{0.2}\text{O}_4$ (open symbols) and patent-type Al-Sb-V-oxide (closed symbols).

this phase was identified (see Fig. 11a) as large crystals giving no EDX metal signal except for antimony. Transmission electron microscopy also shows that the catalyst contains large amounts of alumina and a rutile-related phase, both of which are in the form of very small crystals (see Fig. 11b).

The crystals of $\delta\text{-Al}_2\text{O}_3$ are not more than 5–10 nm in diameter and it is evident in the image in Fig. 12 that the crystals are well aligned, i.e., the whole crystal aggregate is topotactic. X-ray microanalysis gave aluminium exclusively.

The rutile-related phase is identified as such by the ring pattern in Fig. 13a, which is produced by crystal aggregates like the one in Fig. 13b. Since no rings corresponding to su-

perlattice reflections are observed, it is not possible to distinguish between $\text{Sb}_{0.9}\text{V}_{0.9}\text{O}_4$ and $(\text{Al}, \text{Sb}, \text{V})_2\text{O}_4$ by diffraction. As can be seen in high-resolution images (Fig. 13c), the crystals are quite small, i.e., 3–15 nm. In this case, however, no topotaxy is observed, since the phase is probably formed by reaction of several oxide precursors. The X-ray microanalysis reveals the presence of Al, Sb, and V. Unfortunately, the crystals are smaller than the electron beam, so it is not possible to conclude if the aggregate consists of $(\text{Al}, \text{Sb}, \text{V})_2\text{O}_4$ or $\text{Sb}_{0.9}\text{V}_{0.9}\text{O}_4$ with some admixed Al_2O_3 . Attempts to distinguish between $\text{Sb}_{0.9}\text{V}_{0.9}\text{O}_4$ and $(\text{Al}, \text{Sb}, \text{V})_2\text{O}_4$ by direct observation of the two different rutile superstructures have failed; only the basic rutile structure can be seen in high-resolution images (Fig. 13c). Either the crystals are simply too thin for the superstructures to be visible, or these nanocrystals made at 610°C are in fact disordered in contrast to the larger crystals found in the Al-Sb-V-O syntheses prepared at 680°C .

Infrared spectroscopy, however, gave some further indication about the type of rutile phase which is present in the catalyst. Figure 14 shows the infrared spectrum for the catalyst of patent-type together with the spectra for $(\text{Al}, \text{Sb}, \text{V})_2\text{O}_4$ (JN 126) and $\text{Sb}_{0.9}\text{V}_{0.9}\text{O}_4$. In the latter two spectra there are bands in the region below 800 cm^{-1} that are typical of the rutile-type of structure (35–37). For $\text{Sb}_{0.9}\text{V}_{0.9}\text{O}_4$ these bands appear at 345, 545, 670, and 725 (shoulder) cm^{-1} , while for $(\text{Al}, \text{Sb}, \text{V})_2\text{O}_4$ they are at 365, 430, 560, 700, and 765 cm^{-1} . The spectrum of $\text{Sb}_{0.9}\text{V}_{0.9}\text{O}_4$ has two more bands at 880 and 1016 cm^{-1} , which have been previously reported to be from vibration modes involving the 2-coordinated oxygen species which are present in the structure due to it

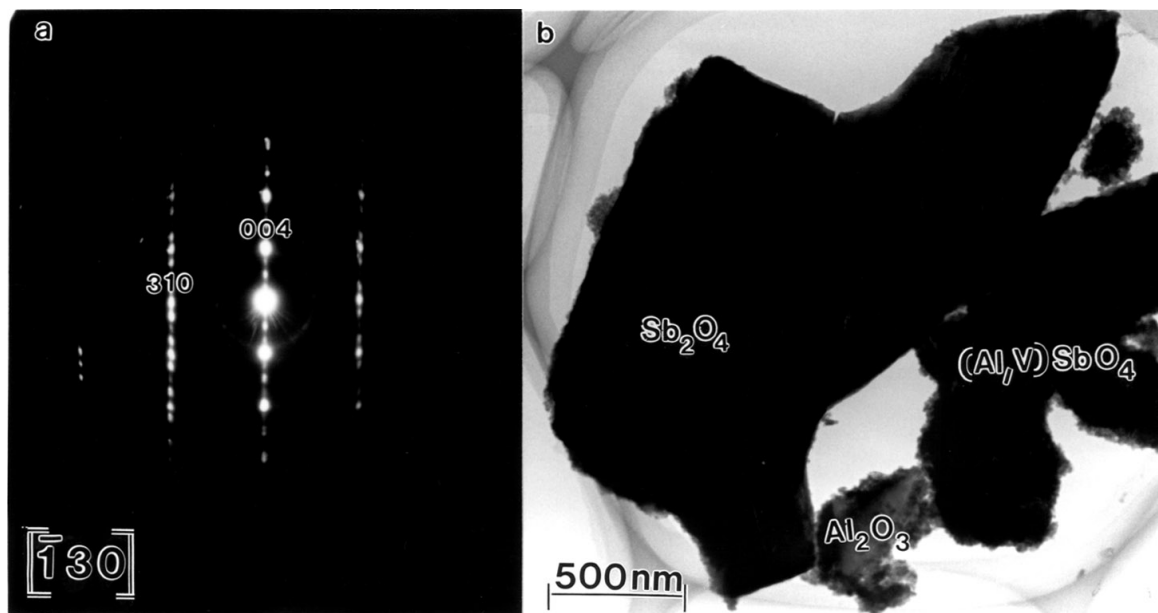


FIG. 11. $\alpha\text{-Sb}_2\text{O}_4$ in the Al-Sb-V-O catalyst of patent-type. (a) Selected area diffraction pattern with $[-1\ 3\ 0]$ as zone axis. (b) Transmission electron micrograph showing big $\alpha\text{-Sb}_2\text{O}_4$ crystals and aggregates consisting of very small crystals of alumina or rutile-type Al-V-Sb-oxide.

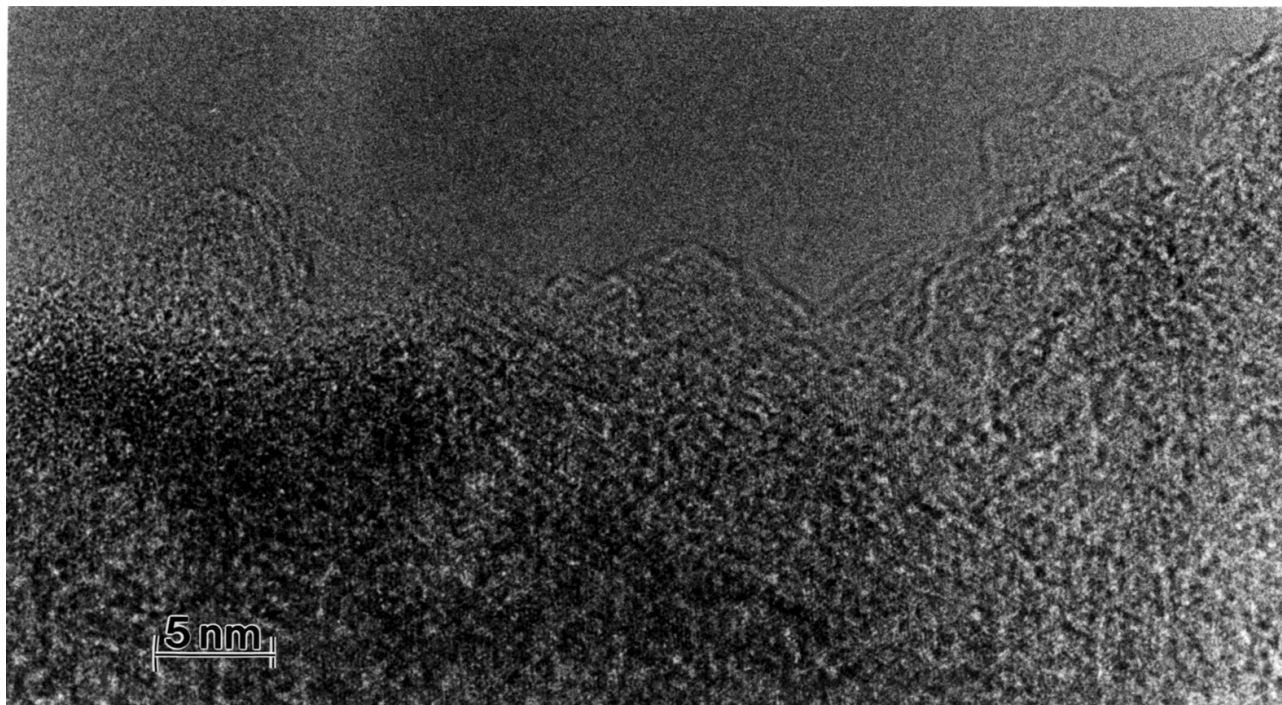


FIG. 12. Transmission electron micrograph of topotactic δ - Al_2O_3 crystals in the Al-Sb-V-O catalyst of patent-type.

being cation deficient (7, 9, 10). It was demonstrated that the intensities of these two bands are proportional to the content of cation vacancies (\square) in $\text{Sb}_{0.9}\text{V}_{0.9+x}\square_{0.2-x}\text{O}_4$ and that the bands are absent in the spectrum of the reduced, defect-free end-composition $\text{Sb}_{0.9}\text{V}_{1.1}\text{O}_4$ (10). There are no infrared bands in the region $850\text{--}1050\text{ cm}^{-1}$ in the spectrum of the catalyst of patent-type, convincingly showing for this sample that $\text{Sb}_{0.9}\text{V}_{0.9}\text{O}_4$ is not the rutile-type structure which is present. The bands that are characteristic for rutile-related structures are not resolved due to contribution from alumina and weak distinct bands from α - Sb_2O_4 (9). However, the spectrum has a resolved band at 360 cm^{-1} and a shoulder at 435 cm^{-1} . These features are in accord with those in spectrum *b* for $(\text{Al}, \text{Sb}, \text{V})_2\text{O}_4$. This agreement points to the rutile phase in the catalyst of patent-type contains aluminium.

Characterisation of samples after use in ammoxidation.

The samples used as catalysts were investigated by X-ray diffraction, FTIR, FT-Raman, and XPS, both as freshly prepared and after use in propane ammoxidation for about 7 h. Neither method revealed any significant change of structure or composition upon use of γ - Al_2O_3 , α - Sb_2O_4 , β - Sb_2O_4 , AlVO_4 , $\text{AlVO}_4/\text{Al}_2\text{O}_3$, AlSbO_4 , β - $\text{Sb}_{1.9}\text{V}_{0.1}\text{O}_4$, $(\text{Al}, \text{Sb}, \text{V})_2\text{O}_4$, and the Al-Sb-V-O catalyst of patent-type. V_2O_5 , on the other hand, was found to be reduced and we have previously reported that V_4O_9 is formed under the present reaction conditions (7, 9). Characterisation with infrared spectroscopy of the $\text{Sb}_{0.9}\text{V}_{0.9}\text{O}_4$ sample after use in

ammoxidation showed that the bands at 880 and 1016 cm^{-1} (cf. Fig. 14) had decreased in intensity relative to the band at 545 cm^{-1} . Using the previously reported correlation between the intensity ratio I_{1015}/I_{545} and the composition of $\text{Sb}_{0.9}\text{V}_{0.9+x}\square_{0.2-x}\text{O}_4$ (10), the observed decrease in the ratio from 0.21 to 0.15 corresponds to reduction of the vanadium and change of the composition from $\text{Sb}_{0.9}\text{V}_{0.9}\square_{0.2}\text{O}_4$ to approximately $\text{Sb}_{0.9}\text{V}_{1.0}\square_{0.1}\text{O}_4$.

For the fresh sample $\text{Sb}_{0.9}\text{V}_{0.9}\text{O}_4/\alpha$ - Sb_2O_4 , with the nominal ratio $\text{Sb}/\text{V} = 2$, the XPS data showed an identical metal ratio. After use of the sample in ammoxidation, the Sb/V ratio was higher (2.7) and the $\text{Sb } 3d_{3/2}$ binding energy had slightly increased (0.1 eV). The changes are not due to experimental error, since similar trends were observed for a whole series of samples with Sb/V ratios within the range 2:1 to 7:1 (7, 9). The trends were explained by enrichment at the $\text{Sb}_{0.9}\text{V}_{0.9}\text{O}_4$ surface with antimony as a result of migration of antimony from α - Sb_2O_4 during the catalytic reaction. Comparison of the infrared spectrum for the fresh $\text{Sb}_{0.9}\text{V}_{0.9}\text{O}_4/\alpha$ - Sb_2O_4 sample with that registered after use in ammoxidation showed less bulk reduction than that observed for pure $\text{Sb}_{0.9}\text{V}_{0.9}\text{O}_4$ without α - Sb_2O_4 .

DISCUSSION

Rutile-Related Phases in the Al-Sb-V-O System

Powder X-ray diffraction shows that the unit cell parameters for $\text{Sb}_{0.9}\text{V}_{0.9}\text{O}_4$ are almost constant in the samples, which indicates a very limited range of composition for

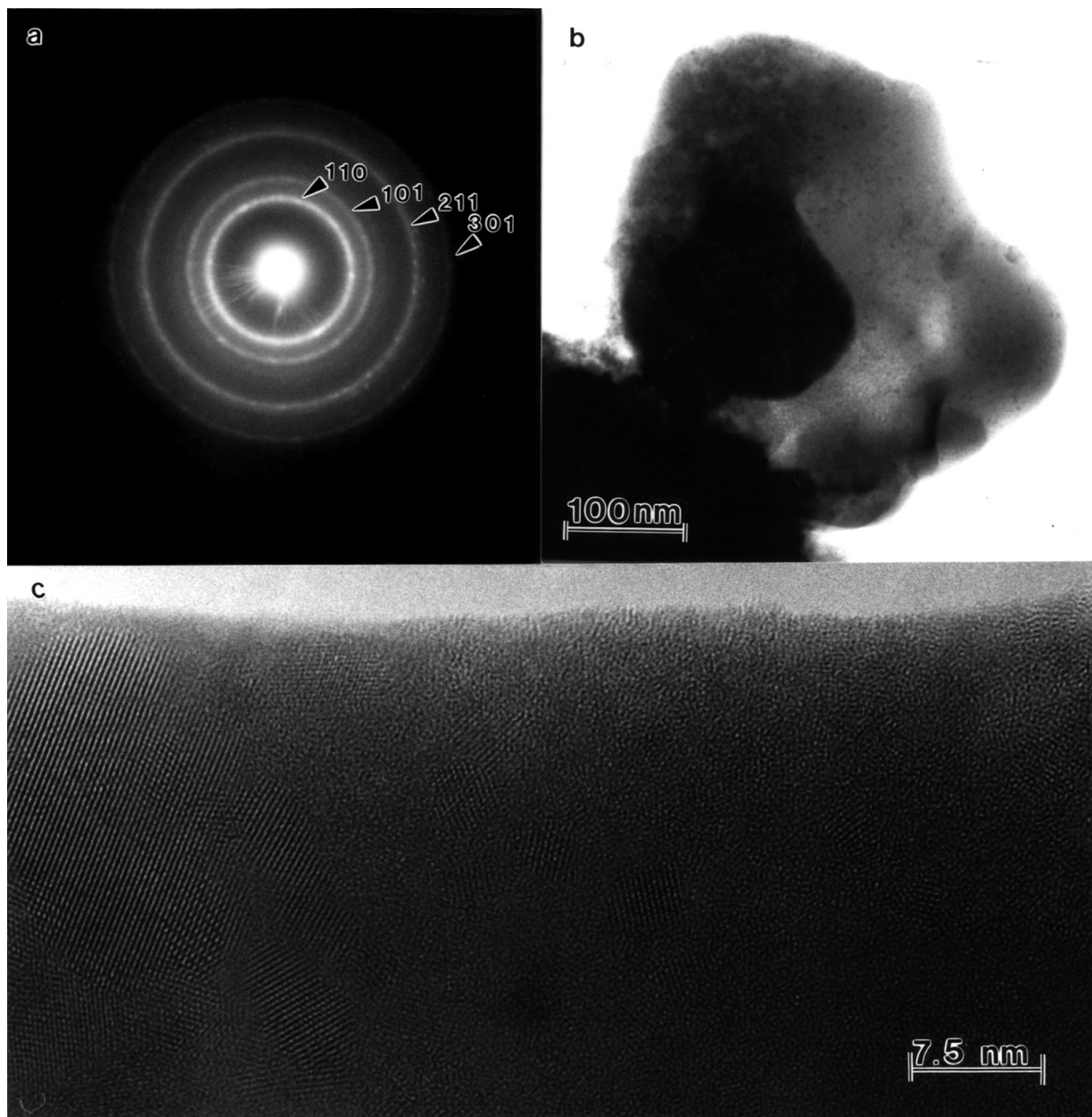


FIG. 13. Rutile-related phase in the Al-Sb-V-O catalyst of patent-type. (a) Selected area electron diffraction pattern of crystal aggregates. Some strong diffraction rings have been indexed using the basic rutile cell. (b) Low-magnification transmission electron micrograph of a crystal aggregate. (c) High-resolution image showing rutile-type crystallites at random orientation.

this phase in the present syntheses performed in air. Energy dispersive X-ray analysis of well-defined $\text{Sb}_{0.9}\text{V}_{0.9}\text{O}_4$ crystals has so far always indicated the absence of aluminium in the crystals, even in cases where a large amount of alumina has been present in the synthesis. Two observations, i.e., the different superlattices in $\text{Sb}_{0.9}\text{V}_{0.9}\text{O}_4$ and $(\text{Al}, \text{Sb}, \text{V})_2\text{O}_4$ as well as the absence of aluminium in clean $\text{Sb}_{0.9}\text{V}_{0.9}\text{O}_4$ crystals, indicate the existence of two distinct rutile-related phases. This indication is somewhat less

obvious from the unit cell data obtained by powder X-ray diffraction (see Table 2). The presence of a gap in the composition between $\text{Sb}_{0.9}\text{V}_{0.9}\text{O}_4$ and $(\text{Al}, \text{Sb}, \text{V})_2\text{O}_4$ (or more specifically $\text{Al}_{0.5}\text{SbV}_{0.5}\text{O}_4$) makes crystal-chemical sense, since $\text{Sb}_{0.9}\text{V}_{0.9}\text{O}_4$ prepared in air has been shown to be essentially a vanadium (4+) compound with a substantial amount of cation vacancies in the structure (6), while the present results indicate that $(\text{Al}, \text{Sb}, \text{V})_2\text{O}_4$ is a vanadium (3+) compound without vacancies. The presence of vacant

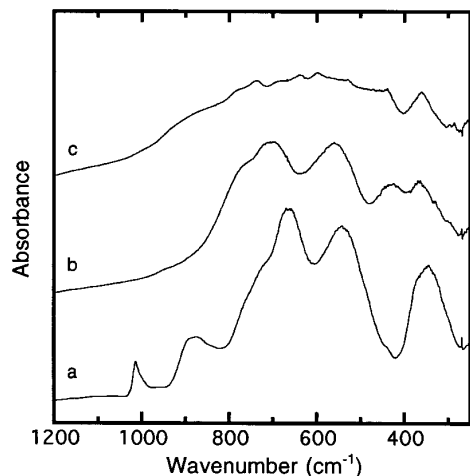


FIG. 14. Infrared spectra of (a) $\text{Sb}_{0.9}\text{V}_{0.9}\text{O}_4$, (b) $(\text{Al}, \text{Sb}, \text{V})_2\text{O}_4$, and (c) Al-Sb-V-O catalyst of patent-type.

metal positions in $\text{Sb}_{0.9}\text{V}_{0.9}\text{O}_4$ and their absence in $(\text{Al}, \text{Sb}, \text{V})_2\text{O}_4$ is clearly demonstrated by the infrared spectra in Fig. 14. The spectrum for the latter phase only has infrared bands that are typical for stoichiometric rutile-type phases, while the former phase exhibits two unique bands at high wavenumbers, which are associated with the presence of metal vacancies (10).

The X-ray data indicate the presence of two separate phases in the trirutile-like series $\text{Al}_{1-x}\text{SbV}_x\text{O}_4$ ($0 < x < 0.5$). This is manifested by the common observation that there are two complete sets of rutile-type diffraction lines on the Guinier films (cf. Table 4), lines which cannot be explained by the presence of $\text{Sb}_{0.9}\text{V}_{0.9}\text{O}_4$. On the other hand, the metal compositions determined by energy dispersive X-ray analysis can be interpreted as a continuous series. There are some subtle variations in the electron diffraction patterns within the series, i.e., the position and sharpness of the superlattice reflections change between crystals. Despite considerable experimental efforts involving the use of electron diffraction and X-ray microanalysis in parallel, it has not been possible to find a straightforward relationship between these diffraction phenomena and composition. This would have allowed us to determine whether two distinct phases exist. Thus, based on the general features of the electron diffraction patterns and the X-ray microanalysis results, we prefer to consider trirutile-type $(\text{Al}, \text{Sb}, \text{V})_2\text{O}_4$, or $(\text{Al}, \text{V})\text{SbO}_4$, as forming a continuous solid solution series from AlSbO_4 to $\text{Al}_{0.5}\text{SbV}_{0.5}\text{O}_4$. In samples with double X-ray diffraction lines for $(\text{Al}, \text{V})\text{SbO}_4$, a bimodal distribution of crystal compositions can be expected. However, the camel-back-shaped distribution can be hard to observe due to the large number of microanalyses on individual crystals which is required to obtain a statistically significant study of a specific sample. In a powder X-ray experiment a very large number of crystals are automatically contributing to

the diffraction pattern. The present syntheses do not correspond to equilibrium conditions due to low temperature and loss of volatile oxides. One possibility is that vanadium-rich $(\text{Al}, \text{V})\text{SbO}_4$ is initially formed, which then decomposes with time to give vanadium-poor $(\text{Al}, \text{V})\text{SbO}_4$.

It has been shown that $\text{Sb}_{0.9}\text{V}_{0.9}\text{O}_4$ formed in air is easily reduced by lowering of the oxygen partial pressure in the surrounding atmosphere during heating (10). In purified nitrogen a phase approaching the end-member composition $\text{Sb}_{0.9}\text{V}_{1.1}\text{O}_4$ is formed. In $\text{Sb}_{0.9}\text{V}_{0.9}\text{O}_4$ tetravalent vanadium predominates, while in reduced $\text{Sb}_{0.9}\text{V}_{1.1}\text{O}_4$, the vanadium is essentially trivalent. Antimony remains pentavalent in the whole series. An interesting implication of the observation that $(\text{Al}, \text{V})\text{SbO}_4$ prepared in an oxidising atmosphere, i.e., air, contains trivalent vanadium is that this phase ought to be less sensitive to bulk reduction when the oxygen partial pressure is lowered, since vanadium is already fully reduced. Divalent vanadium is not usually formed in catalytic oxidations (24). Preliminary experiments, where $(\text{Al}, \text{V})\text{SbO}_4$ was first prepared in air and then a part of the sample was heated in purified nitrogen, have confirmed the predicted behaviour. The two resulting $(\text{Al}, \text{V})\text{SbO}_4$ materials exhibited very small differences in unit cell parameters, in contrast to that observed for $\text{Sb}_{0.9}\text{V}_{0.9}\text{O}_4$ and $\text{Sb}_{0.9}\text{V}_{1.1}\text{O}_4$ prepared in a similar fashion (10).

The compound $(\text{Al}, \text{V})\text{SbO}_4$ reported here exhibits interesting analogies with another substance of interest in catalytic oxidation, i.e., FeSbO_4 , which is selective for oxidation and ammoxidation of propylene (38, 39). Both phases seem to be of $\text{A}^{\text{III}}\text{B}^{\text{V}}\text{O}_4$ stoichiometry, but despite the one-to-one ratio between trivalent and pentavalent cations both exhibit a threefold superstructure when examined by electron diffraction, but only the basic rutile structure when investigated by powder diffraction methods (33, 40).

Role of the Various Cation Centres for Propane Ammoxidation

It is by now well-established that propylene is a major intermediate in propane ammoxidation to acrylonitrile (7, 9, 27, 31). The data in Figs. 6, 7, and 9 show for selected samples both the ability of the samples to initially transform propane to propylene as well as the ability of the samples to transform the formed propylene further to acrylonitrile. This type of data is suited for rationalisation of the catalytic role of the various cation centres which are present in Al-Sb-V-oxides.

Comparison of the catalytic data in Fig. 6 for V_2O_5 , $\gamma\text{-Al}_2\text{O}_3$, and the Sb_2O_4 polymorphs clearly shows that both V_2O_5 and Sb_2O_4 catalyse initially, at 5% propane conversion, the formation of propylene from propane with similar selectivity (35–50%). The activity of V_2O_5 , however, is approximately 20 times higher per unit surface area than it is for the Sb_2O_4 polymorphs. Moreover, the alumina shows very low activity for propane activation and converts

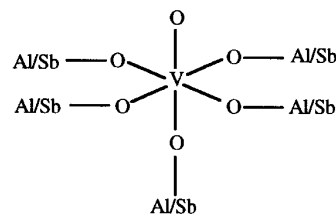
propane mainly to C_1 and C_2 degradation products, which is in line with the fact that alumina is acidic and a medium-activity matrix in cracking catalysts (41). The main conclusion that can be drawn from the data in Fig. 6 is that V-sites are primary adsorption sites for propane and are the most active for the oxidative dehydrogenation of form propylene. With increase in propane conversion, however, the propylene is degraded.

Initially, i.e., at 5% conversion, the selectivities to propylene and acrylonitrile are almost identical over both Sb_2O_4 (Fig. 6) and $AlSbO_4$ (Fig. 7), while the specific activity of the former oxide is higher. These data imply that in $AlSbO_4$ it is the Sb-sites which are the most active and that the Al-sites are unable to insert nitrogen to the propylene or the allylic intermediate which is formed at an Sb-moiety. The data in Fig. 7 show that $Sb_{0.9}V_{0.9}O_4$ and $AlVO_4$, compared with $AlSbO_4$, are considerably more active and also more selective to acrylonitrile formation. Furthermore, the selectivity values for propylene formation over the two latter oxides are similar at each conversion level and so are the selectivity values for the formation of acrylonitrile. These data clearly show that in $Sb-V-O$ and $Al-V-O$ structures it is the vanadium site that is active and is participating in the insertion of nitrogen. The contribution to the nitrogen insertion from the Sb-sites in $Sb_{0.9}V_{0.9}O_4$, likewise the Al-sites in $AlVO_4$, obviously seems to be negligible. The reaction rate over $Sb_{0.9}V_{0.9}O_4$ and $AlVO_4$ is similar, indicating that Sb-sites, likewise Al-sites, are not reoxidation sites. This function, therefore, has to be performed by a V-moiety.

Despite the observation that Sb-sites have some activity for propylene and acrylonitrile formation, the discussion so far has shown that in oxide matrices with both vanadium and antimony sites it is the former that determine the gross performance. The vanadium centres are active for propane activation, dehydrogenation, nitrogen insertion, and reoxidation, leading to formation of propylene and acrylonitrile. This result seems limited to the present system with vanadium, since in mixed oxides with two or more cation types, generally different catalyst functions have been associated with different types of cation (28, 37, 42).

A point that remains to be answered concerns the role of aluminium and antimony in the $Al-Sb-V$ -oxides for propane ammoxidation. In this regard, some valuable information can be extracted from Figs. 6, 7, and 9. If the data for the V-containing oxides are compared, it is seen that the specific activity decrease with decrease in vanadium content of the oxide, i.e., in the order $V_2O_5 > Sb_{0.9}V_{0.9}O_4 \approx AlVO_4 > Sb_{0.9}V_{0.9}O_4/\alpha-Sb_2O_4 > \beta-Sb_{1.9}V_{0.1}O_4 \approx (Al, Sb, V)_2O_4$. The sum of the selectivities to propylene and acrylonitrile at 5% propane conversion is in the range 55–70% for the same oxides and, conversely to the activity, the selectivity sum increases with decrease in vanadium content. The same trend is valid for the 15% conversion level, where the sum of the selectivities is 36% for V_2O_5 and more

than 55% for $\beta-Sb_{1.9}V_{0.1}O_4$ and $(Al, Sb, V)_2O_4$. More striking is the concurrent trend for the selectivity to acrylonitrile, which at the 15% conversion level increases from 9% for V_2O_5 to about 15% for $Sb_{0.9}V_{0.9}O_4$ and $AlVO_4$ and to 30–40% for $\beta-Sb_{1.9}V_{0.1}O_4$ and $(Al, Sb, V)_2O_4$. Consequently, the present data clearly show that the role of the aluminium and antimony concerning catalysis on $Al-Sb-V$ -oxides is to create isolation of V-centres. Site isolation is necessary to avoid degradation and have a catalyst that is selective for acrylonitrile formation. Thus, the active site is possibly of the type:



SCHEME 1

On the above type of site, the whole series of transformations from propane to acrylonitrile can be accomplished, possibly with desorption and readsorption of formed propylene. It cannot be excluded that a dimeric $V-O-V$ centre is involved, but the present results show that polymeric V-centres give degradation products. Isolation of V-centres at the atomic level is necessary, as is obvious comparing the data in Fig. 7 for the $AlVO_4$ and $AlVO_4/Al_2O_3$ samples. Dispersion of $AlVO_4$ on alumina does not give higher selectivity to acrylonitrile, though a minor increase in the selectivity to propylene was obtained. Comparison of the data for $Sb_{0.9}V_{0.9}O_4$ (Fig. 7) and $Sb_{0.9}V_{0.9}O_4/\alpha-Sb_2O_4$ (Fig. 9) shows the latter catalyst to give considerably more of acrylonitrile. This is, however, not due to dispersion of $Sb_{0.9}V_{0.9}O_4$ on $\alpha-Sb_2O_4$, but has been shown to be caused by dilution and isolation of surface V-centres due to migration of antimony species from $\alpha-Sb_2O_4$ (7, 9, 29).

The present result, showing the importance of isolation of V-centres in $Al-Sb-V$ -oxides for obtaining partial oxidation, indeed, is a new example of the validity of the site isolation theory that was put forward by Callahan and Grasselli (43). The necessity of having structurally isolated sites with a suitable number of oxygen species of appropriate metal-oxygen bond strength has previously been shown to be crucial also for propylene ammoxidation over the $U-Sb$ -oxide system (44, 45). In this system USb_3O_{10} is selective and has U-sites which are fully surrounded by Sb atoms.

Active Phase in an Al-Sb-V-O Preparation of Patent Type

Except for the lines from $\alpha-Sb_2O_4$, the patent-type of catalyst was largely found to be X-ray amorphous. Transmission electron microscopy showed additionally the presence

of alumina and a rutile-related phase in the form of polycrystalline aggregates (Figs. 11b, 12, and 13c). Though electron diffraction (Fig. 13a) and EDX analysis did not allow the distinction between $\text{Sb}_{0.9}\text{V}_{0.9}\text{O}_4/\text{Al}_2\text{O}_3$ and $(\text{Al}, \text{Sb}, \text{V})_2\text{O}_4$, infrared spectroscopy (Fig. 14) clearly revealed the rutile-phase in this catalyst to be free of cation vacancies, i.e., not to be $\text{Sb}_{0.9}\text{V}_{0.9}\text{O}_4$. In support of the active phase being $(\text{Al}, \text{Sb}, \text{V})_2\text{O}_4$, i.e., $\text{Al}_{1-x}\text{SbV}_x\text{O}_4$ with $0 < x < 0.5$, are the activity data in Figs. 9 and 10 which show almost identical catalytic performance for the $(\text{Al}, \text{Sb}, \text{V})_2\text{O}_4$ sample and the catalyst of patent-type with excess alumina. Moreover, the composition of the latter places it in the lower right corner in the triangle in Fig. 1, showing the field of formation for $(\text{Al}, \text{Sb}, \text{V})_2\text{O}_4$. This fact is another support for the notion that the patent-type catalyst, besides alumina, consists of a rutile-related phase $(\text{Al}, \text{Sb}, \text{V})_2\text{O}_4$. Our experiments have shown that an excess of alumina is required to form $(\text{Al}, \text{Sb}, \text{V})_2\text{O}_4$ at 680°C and that the excess alumina promotes the formation of the end-composition $(\text{Al}, \text{Sb}, \text{V})_2\text{O}_4(\text{I})$ or $\approx \text{Al}_{0.8}\text{Sb}_{1.0}\text{V}_{0.2}\text{O}_4$ (Fig. 1). A low calcination temperature favors the more vanadium-rich end-composition $(\text{Al}, \text{Sb}, \text{V})_2\text{O}_4(\text{II})$ or $\approx \text{Al}_{0.5}\text{Sb}_{1.0}\text{V}_{0.5}\text{O}_4$; e.g., heating of the sample JN 126 at 900°C (Fig. 2) produced pure $(\text{Al}, \text{Sb}, \text{V})_2\text{O}_4$ with a vanadium content between the two end-compositions, but heating at 680°C gave an impure sample with vanadium-rich $(\text{Al}, \text{Sb}, \text{V})_2\text{O}_4(\text{II})$ together with $\text{Sb}_{0.9}\text{V}_{0.9}\text{O}_4$, $\alpha\text{-Sb}_2\text{O}_4$, and alumina (cf. Fig. 1). Considering that the patent-type of catalyst was calcined at somewhat lower temperature (610°C) as compared to the samples that were used for the determination of the regions of phase formation (680°C to increase crystallinity), it seems reasonable that the composition of the active phase can be given as $\text{Al}_{1-x}\text{SbV}_x\text{O}_4$ where $0.2 < x < 0.5$. A lower value of x possibly improves the isolation of V-centres, which is in favour of the selectivity toward acrylonitrile. The activity, conversely, decreases with decrease in V-content. An intermediate vanadium content, therefore, should give an optimal yield of the nitrile.

CONCLUSIONS

Calcination at 680°C in air of mixtures with $\text{Al}(\text{OH})_3$, Sb_2O_3 , and V_2O_5 was shown to give, besides the simple oxides with one type of metal ion, the following phases: AlVO_4 , $\text{Sb}_{0.9}\text{V}_{0.9}\text{O}_4$, and a trirutile-like series $\text{Al}_{1-x}\text{SbV}_x\text{O}_4$ with $0 < x < 0.5$. This series is described here for the first time and was identified as the best material for acrylonitrile formation among the phases belonging to the Al-Sb-V-O system. Characterisation of an Al-Sb-V-O sample with the atomic ratios $\text{Al}:\text{Sb}:\text{V} = 21:5:1$, which was prepared according to procedures described in patents (5), allowed the identification of $\text{Al}_{1-x}\text{SbV}_x\text{O}_4$ as the active phase. One role of the alumina in excess is to promote the formation of $\text{Al}_{1-x}\text{SbV}_x\text{O}_4$, thereby preventing the formation of less

selective $\text{Sb}_{0.9}\text{V}_{0.9}\text{O}_4$. Without excess alumina, the formation of the latter phase seems kinetically favoured.

Comparison of the performances for propane ammoxidation of simple and complex oxides belonging to the Al-Sb-V-O system revealed that in the oxides with more than one type of metal ion it is the V-sites, when present, which determine the catalyst performance. The V-sites initially give propylene, which then goes to either acrylonitrile or waste products. For obtaining a catalyst that is selective to acrylonitrile, it is necessary to have structurally isolated V-centres that are surrounded by Al and/or Sb. This is a new example of the validity of the site isolation theory as formulated by Callahan and Grasselli more than 30 years ago (43).

ACKNOWLEDGMENTS

Financial support from the Swedish National Research Council for Engineering Sciences (TFR), the Swedish Natural Science Research Council (NFR), and the Ministerio Español de Educación y Ciencia is gratefully acknowledged.

REFERENCES

1. Wittcoff, H. A., *CHEMTEC* **20**, 48 (1990).
2. Malow, M., in "Handbook of Chemicals Production Processes" (R. A. Meyers, Ed.), Ch. 1.9. McGraw-Hill, New York, 1986.
3. Newsletter, *Appl. Catal.* **67**, N5 (1990).
4. US Patents 4,760,154 (1988); 4,835,125 (1989); 4,837,191 (1989); 4,843,055 (1989); assigned to the Standard Oil Company (Ohio).
5. US Patents 4,746,641 (1988); 4,784,979 (1988); 4,788,317 (1988); 4,871,706 (1989); 4,877,764 (1989); 4,879,264 (1989); assigned to the Standard Oil Company (Ohio).
6. Hansen, S., Ståhl, K., Nilsson, R., and Andersson, A., *J. Solid State Chem.* **102**, 340 (1993).
7. Nilsson, R., Lindblad, T., Andersson, A., Song, C., and Hansen, S., in "New Developments in Selective Oxidation II" (V. Cortéz Corberán and S. Vic Bellón, Eds.), Studies in Surface Science and Catalysis, Vol. 82, p. 293. Elsevier, Amsterdam, 1994.
8. Landa-Cánovas, A. R., Nilsson, J., Hansen, S., Ståhl, K., and Andersson, A., in "Electron Microscopy 1994" (B. Jouffrey and C. Colliex, Eds.), Vol. 2B, p. 873. Les Editions de Physique, Paris, 1994.
9. Nilsson, R., Lindblad, T., and Andersson, A., *J. Catal.* **148**, 501 (1994).
10. Landa-Cánovas, A., Nilsson, J., Hansen, S., Ståhl, K., and Andersson, A., *J. Solid State Chem.* **116**, 369 (1995).
11. Brandt, K., *Ark. Kemi* **17**, 1 (1943).
12. Baran, E. J., and Botto, I. L., *Monatsh. Chem.* **108**, 311 (1977).
13. Birchall, T., and Sleight, A. W., *Inorg. Chem.* **15**, 868 (1976).
14. Berry, F. J., Brett, M. E., and Patterson, W. R., *J. Chem. Soc. Dalton Trans.*, 9 (1983).
15. Bachmann, H. G., Ahmed, F. R., and Barnes, W. H., *Z. Kristallogr.* **115**, 110 (1961).
16. Stewart, D. J., Knop, O., Ayasse, C., and Woodhams, F. W. D., *Can. J. Chem.* **50**, 690 (1972).
17. Thornton, G., *Acta Cryst.* **B33**, 1271 (1977).
18. Rogers, D., and Skapski, A. C., *Proc. Chem. Soc.*, 400 (1964).
19. Satterfield, C. N., "Heterogeneous Catalysis in Industrial Practice," 2nd ed., pp. 114-120. McGraw-Hill, New York, 1991.
20. Teller, R. G., Antonio, M. R., Brazdil, J. F., and Grasselli, R. K., *J. Solid State Chem.* **64**, 249 (1986).
21. Andersson, A., Andersson, S. L. T., Centi, G., Grasselli, R. K., Sanati, M., and Trifirò, F., in "Proceedings, 10th International Congress on Catalysis, Budapest, 1992" (L. Guzzi, F. Solymosi, and P. Tétényi,

- Eds.), *Studies in Surface Science and Catalysis*, Vol. 75, p. 691. Elsevier, Amsterdam, 1993.
22. Schwarzmann, E., Rumpel, H., and Berndt, W., *Z. Naturforsch.* **32** b, 617 (1977).
 23. Rumpel, H., Berndt, W., Adam, K., and Schwarzmann, E., *Z. Naturforsch.* **33** b, 39 (1978).
 24. Andersson, A., Bovin, J.-O., and Walter, P., *J. Catal.* **98**, 204 (1986).
 25. Reid, A. F., and Sabine, T. M., *J. Solid State Chem.* **2**, 203 (1970).
 26. Cody, C. A., DiCarlo, L., and Darlington, R. K., *Inorg. Chem.* **18**, 1572 (1979).
 27. Centi, G., Grasselli, R. K., Patanè, E., and Trifirò, F., in "New Developments in Selective Oxidation" (G. Centi and F. Trifirò, Eds.), *Studies in Surface Science and Catalysis*, Vol. 55, p. 515. Elsevier, Amsterdam, 1990.
 28. Grasselli, R. K., Centi, G., and Trifirò, F., *Appl. Catal.* **57**, 149 (1990).
 29. Nilsson, R., Lindblad, T., and Andersson, A., *Catal. Lett.* **29**, 409 (1994).
 30. JCPDS International Centre for Diffraction Data, "Powder Diffraction File," Swarthmore, PA, 1991.
 31. Catani, R., Centi, G., Trifirò, F., and Grasselli, R. K., *Ind. Eng. Chem. Res.* **31**, 107 (1992).
 32. Shannon, R. D., *Acta Crystallogr. Sect. A* **32**, 751 (1976).
 33. Hansen, S., Landa-Cánovas, A., Ståhl, K., and Nilsson, J., *Acta Crystallogr. Sect. A* **51**, 514 (1995).
 34. Lippens, B. C., and de Boer, J. H., *Acta Crystallogr.* **17**, 1312 (1964).
 35. Rocchiccioli-Deltcheff, C., Dupuis, T., Franck, R., Harmelin, M., and Wadier, C., *C. R. Acad. Sci. Paris Ser. B* **270**, 541 (1970).
 36. Husson, E., Repelin, Y., Brusset, H., and Cerez, A., *Spectrochim. Acta* **35A**, 1177 (1979).
 37. Carbucicchio, M., Centi, G., and Trifirò, F., *J. Catal.* **91**, 85 (1985).
 38. Aso, I., Furukawa, S., Yamazoe, N., and Seiyama, T., *J. Catal.* **64**, 29 (1980).
 39. Teller, R. G., Brazdil, J. F., and Grasselli, R. K., *J. Chem. Soc. Faraday Trans. 1* **81**, 1693 (1985).
 40. Berry, F. J., Holden, J. G., and Loretto, M. H., *J. Chem. Soc. Faraday Trans. 1* **83**, 615 (1987).
 41. Scherzer, J., *Catal. Rev. Sci. Eng.* **31**, 215 (1989).
 42. Burrington, J. D., Kartisek, C. T., and Grasselli, R. K., *J. Catal.* **87**, 363 (1984).
 43. Callahan, J. L., and Grasselli, R. K., *AIChE J.* **9**, 755 (1963).
 44. Grasselli, R. K., and Suresh, D. D., *J. Catal.* **25**, 273 (1972).
 45. Grasselli, R. K., and Burrington, J. D., in "Advances in Catalysis" (D. D. Eley, H. Pines, and P. B. Weisz, Eds.), Vol. 30, p. 133. Academic Press, New York, 1981.